Received 10 October 2019; revised 13 December 2019; accepted 11 January 2020. Date of publication 14 January 2020; date of current version 31 January 2020. The review of this article was arranged by Editor K. Shenai.

Digital Object Identifier 10.1109/JEDS.2020.2966680

A Silicon Carbide 256 Pixel UV Image Sensor Array Operating at 400 °C

SHUOBEN HOU, MUHAMMAD SHAKIR, PER-ERIK HELLSTRÖM (Member, IEEE), BENGT GUNNAR MALM (Senior Member, IEEE), CARL-MIKAEL ZETTERLING (Senior Member, IEEE), AND MIKAEL ÖSTLING (Fellow, IEEE)

School of Electrical Engineering and Computer Science, KTH Royal Institute of Technology, 16440 Kista, Sweden

CORRESPONDING AUTHOR: S. HOU (e-mail: shuoben@kth.se)

This work was supported in part by the "Working on Venus" Project from Knut and Alice Wallenberg Foundation and in part by the "CMP Lab" Project from the Swedish Foundation for Strategic Research.

This article has supplementary downloadable material available at http://ieeexplore.ieee.org, provided by the author.

ABSTRACT An image sensor based on wide band gap silicon carbide (SiC) has the merits of high temperature operation and ultraviolet (UV) detection. To realize a SiC-based image sensor the challenge of opto-electronic on-chip integration of SiC photodetectors and digital electronic circuits must be addressed. Here, we demonstrate a novel SiC image sensor based on our in-house bipolar technology. The sensing part has 256 (16×16) pixels. The digital circuit part for row and column selection contains two 4-to-16 decoders and one 8-bit counter. The digital circuits are designed in transistor-transistor logic (TTL). The entire circuit has 1959 transistors. It is the first demonstration of SiC opto-electronic on-chip integration. The function of the image sensor up to 400 °C has been verified by taking photos of the spatial patterns masked from UV light. The image sensor would play a significant role in UV photography, which has important applications in astronomy, clinics, combustion detection and art.

INDEX TERMS Silicon carbide (SiC), image sensor, ultraviolet (UV), photodiode, high temperature, bipolar junction transistor (BJT), transistor-transistor logic (TTL).

I. INTRODUCTION

Many applications, not limited to astronomy, clinics, combustion detection and art, have a strong demand in UV-only photography [1], [2], [3]. Some of them also request the durability of the hardware (e.g., image sensor) in extremely high temperature environments [4], [5], [6], [7], [8]. Conventional image sensors applied in ultraviolet (UV) photography are Si-based in combination with external band-pass filters [9], [10]. Since there is no band-pass filter that can totally reject visible and infrared light, a pure UV image of any object cannot be achieved. Moreover, Si technology has an operational temperature limitation of 300 °C. A high leakage current also degrades the signal-to-noise ratio (SNR) of the photodetectors. On the contrary, SiC, as a wide band gap material, is ideal for UV-only detection in a wider temperature window [11]. SiC is naturally transparent to visible and infrared light. SiC electronics are also superior in high temperature operations. The junction is neither affected by the high ambient temperature nor the infrared thermal emission from the background. SiC photodetectors and integrated circuits (IC) have been under development since 1990s [12], [13], however, no work in on-chip integration of the two parts has ever been reported to produce an image sensor.

There are several device options, such as MOSFET [14], [15], [16], JFET [17], [18] and BJT [19], [20], [21], in the SiC circuit design for $>$ 400 °C applications. BJT is more thermally stable compared to MOSFET. The gate dielectric of MOSFET has durability issues under a high temperature stress and it leads to a threshold voltage shift over time [22]. The most complex SiC-based circuit has been realized in CMOS with 1398 transistors, but the maximum operational temperature is only 300 °C [23].

Our preliminary works have shown the high temperature performance of discrete UV-only SiC photodetectors (up to 550 °C) [24], [25], [26] and BJT (up to 400 °C) as a switch controlling a photodiode [27]. We have also presented our

This work is licensed under a Creative Commons Attribution 4.0 License. For more information, see http://creativecommons.org/licenses/by/4.0/

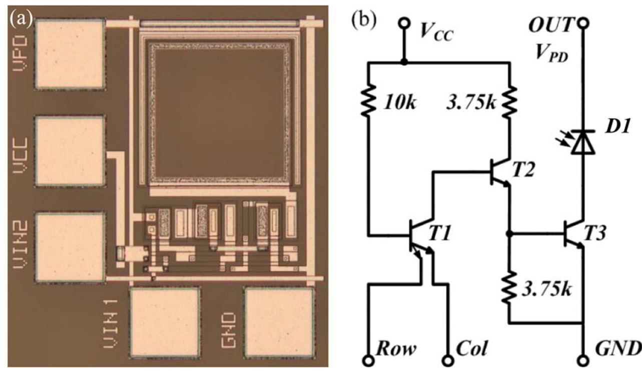

FIGURE 1. (a) Microscope image and (b) circuit diagram of the discrete 3-T bipolar pixel sensor.

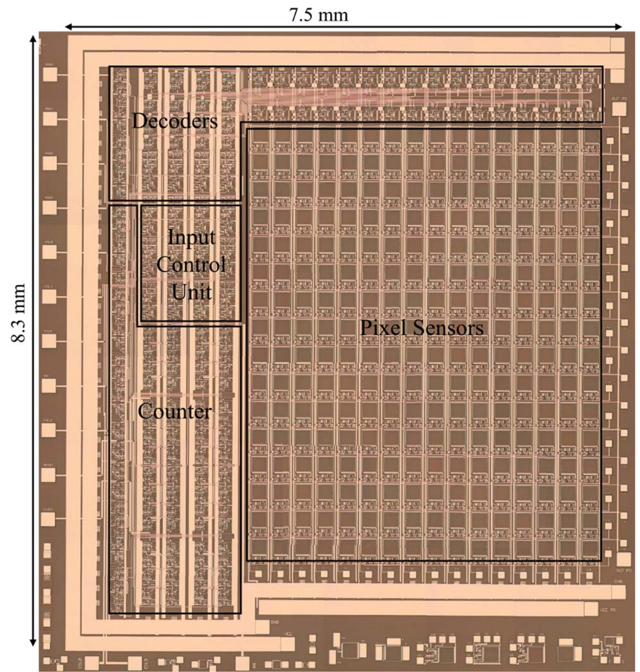

FIGURE 2. Microscope image of the entire image sensor circuit. It has a total area of 62.3 mm^2. The four main building blocks are 4-to-16 decoder, 8-bit counter, input control unit (2×4 tri-state buffer array) and 16×16 pixel sensors.

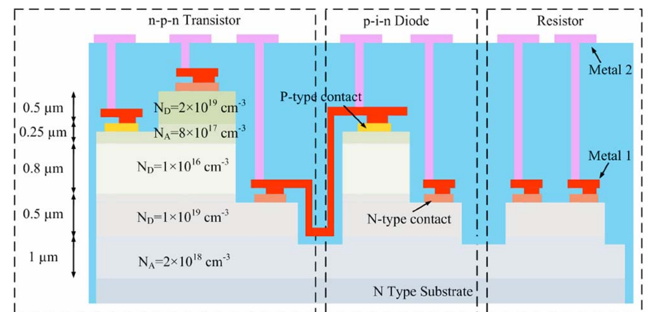

FIGURE 3. Schematic cross-section of the monolithically fabricated devices, including the transistor, photodiode and resistor.

work on a TTL process design kit (PDK) demonstrating the functionality of basic digital circuits up to 500 °C [28]. Here, our in-house processing flow for SiC bipolar technology has been optimized to achieve a higher yield in both device level and circuit level [29] so that an image sensor is demonstrated. The pixel sensor is realized in a bipolar 3-transistor (3-T) design. The image sensor circuit consists of 256 (16×16) pixel sensors, two 4-to-16 decoders and one 8-bit counter. The pixel sensor is characterized from room temperature (RT) to 500 °C. The functionality of the image sensor up to 400 °C is verified by taking photos of spatial patterns masked from a UV LED.

II. DESIGN AND FABRICATION

The microscope image and the circuit diagram of the discrete bipolar 3-T pixel sensor are shown in Fig. 1 (a) and (b) respectively. D1 is the photodiode. It has the same layout as our former design in [24]. T1 is the input stage transistor with two emitter terminals as row and column (Col) inputs. T3 is the switching transistor.

The microscope image of the fabricated image sensor is shown in Fig. 2. It has 16×16 pixel sensors. Its digital circuit is composed of two 4-to-16 decoders, one 8-bit counter and an input control unit of a 2×4 tri-state buffer array. The image sensor has 1959 transistors in total and the whole layout has an area of 62.3 mm^2. The circuits are built from standard discrete cells (inverter, buffer, AND, XOR and D flip-flop) selected from our TTL PDK [28]. The schematic diagrams of the digital circuits are shown in the Supplementary Material of this paper. The input control unit divides the inputs to the decoders by direct probing (enable=0) or clock input at the counter (enable=1). The reason to add the input control unit is to test the image sensor with decoders only in case the counter fails. The outputs from the counter and the decoders are designed to turn each pixel sensor ON sequentially from top left to bottom right.

The cross-section of the on-chip devices, including the bipolar transistor, epitaxial UV photodiode and resistor is shown in Fig. 3. The figure also shows the connection of the metal line between the transistor and photodiode in the pixel sensor design.

The performance uniformity and the yield of the devices and circuits have been upgraded from our former work by improving the processing flow [29]. The processing started from 4H-SiC 100 mm substrates with epitaxial layers. The mesas of the devices were etched in three reactive ion etching (RIE) steps. A high flow of SF_6 (30 sccm) was applied in the RIE to solve the photoresist re-deposition issue [29]. A sloped mesa sidewall and a uniform etching speed was achieved. A thermal oxidation layer was grown in dry O_2 at 1100 °C for 1 hour and removed thereafter to smooth the SiC surface. A passivation PECVD oxide of 100 nm was first deposited and then annealed in N_2O at 1250 °C for 1 hour to further reduce the etching damages.

The n-type ohmic contact was made by a Ni-based self-aligned two-step-annealing process [30]. The p-type Ohmic contact was made by a Ni-Al-based semi-self-aligned process [31]. The interconnect dielectric was PECVD oxide and the interconnect metal was sputtered TiW and Al. The TiW layer was 100 nm and it served as a diffusion barrier to prevent the Al from diffusing into, reacting with and degrading the contact. Chemical-mechanical polishing (CMP) was added to the processing flow because the circuit layout required a two-level metal interconnect design to reduce the area consumption. The CMP process was employed after depositing a thick oxide layer on the first metal layer (M1, 1 µm) to planarize the device topography (4 µm). Without CMP a clear pattern on the second metal layer (M2) cannot be shaped because the topography exceeds the depth of focus of the lithography machine. It leads to short circuit between the metal lines following an incomplete photoresist developing and metal etching process [29]. M2 had a thick Al layer of 2 µm to carry the high current from the TTL circuits, especially at the power supply and ground terminals.

III. MEASUREMENT SETUP

The UV LED used for illumination was SOLIS-365C from Thorlabs. The LED had an aperture diameter of 48.3 mm, a wavelength of 365 nm (bandwidth 10 nm) and a maximum optical power of 4 W (0.22 W/cm^2). The intensity of the LED was controlled by a manual current driver (DC20, Thorlabs). The UV light was illuminated on the pixel sensor and image sensor continuously for all the optical measurements in this paper. The maximum optical power was used for the discrete pixel sensors but ∼10 times reduced optical power was used for the whole image sensor. The parameter analyser for current-voltage measurements was Keithley 4200 SCS. The input of the pixel sensor, digital circuits and image sensor in the transient response measurement was programmed with a FPGA (Altera DE2). The voltage supply (V_{CC}) of all the digital circuits was always set at 15 V. The high temperature measurement was performed on a probe station having a ceramic hot chuck with a temperature control. The actual chuck temperature was always monitored by an infrared thermometer and an on-chip SiC diode temperature sensor [32].

IV. RESULTS AND DISCUSSIONS

A. PIXEL SENSORS

The DC characteristics of the pixel sensor is shown in Fig. 4 (a). The row input is biased at 10 V and the column input is swept from 0 V to 10 V. The pixel is switched ON when both inputs are at high voltage since T3 works in its saturation region (V_B =∼3 V) [27]. With either input at low voltage, the photocurrent generated in the photodiode is switched OFF since T3 works in its cut-off region (V_B =∼0 V) [27]. The transfer voltage is around 5.5 V at RT and it has a temperature dependency of ∼5 mV/°C due to the shift of forward voltage drop of both T1 and T3. The OFF-state current of the pixel is half of the ON-state current. The source of the OFF-state current is a "hidden" photodiode under the designed photodiode. As shown in Fig. 3, the output of the pixel sensor (cathode of the photodiode) is not only connected to the designed photodiode but also a p-n junction formed by the collector and isolation layers. The collector-isolation p-n junction can also generate a photocurrent once the isolation layer is biased. The collector-isolation diode is always "ON" no matter if T3 is turned ON or OFF. The value of the photocurrent from the collector-isolation diode is similar to that from the

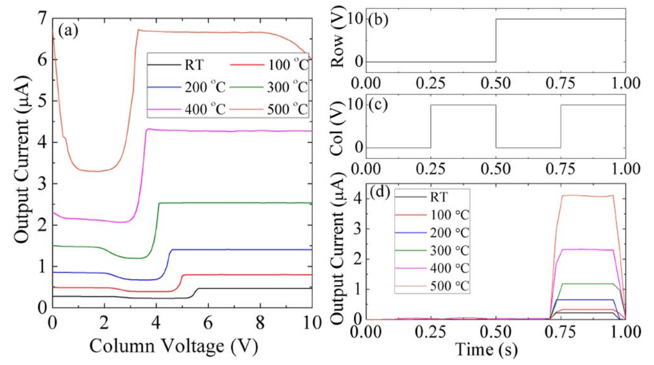

FIGURE 4. (Left) (a) The output current as a function of the column input voltage of the discrete pixel sensor from RT to 500 °C. The row input voltage is biased at 10 V. (Right) Transient response of the discrete pixel sensor from RT to 500 °C. (b) Waveform of the row input. (c) Waveform of the column input. (d) Waveform of the output current. With both input voltages at "HIGH" (10 V) the photocurrent from the photodiode is switched ON. Note that the OFF-state current is subtracted in (d), not in (a).

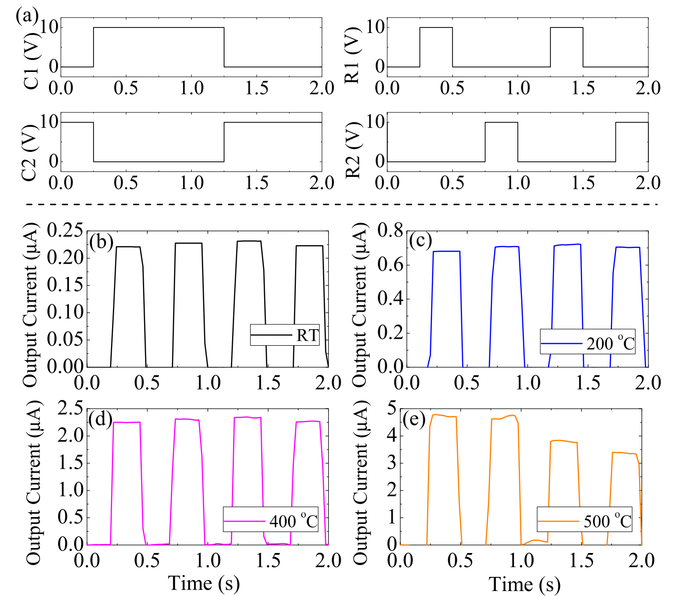

FIGURE 5. Transient response of the 2×2 pixel sensor array from RT to 500 °C. (a) Waveforms of the inputs. (b), (c), (d) and (e) Waveforms of the output at RT, 200 °C, 400 °C and 500 °C. Each pixel is switched ON in sequence with a total-OFF-state in between. Note that the OFF-state current is subtracted in (b)-(e).

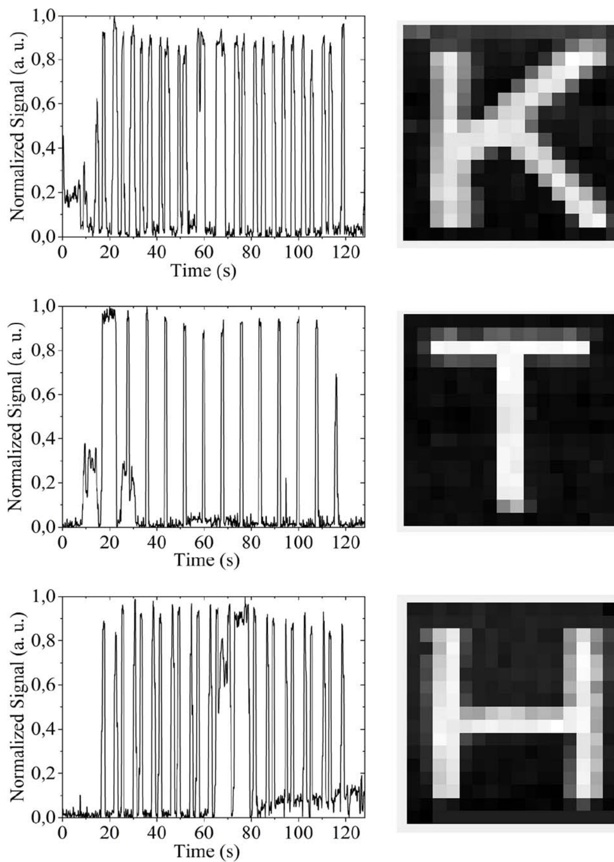

FIGURE 6. Normalized signals read-out from the image sensor and the 16×16 resolution grey-scale images converted from the signals at RT. The light illuminated on the pixel sensors of the image sensor has spatial patterns ("K", "T", "H") masked from a UV LED.

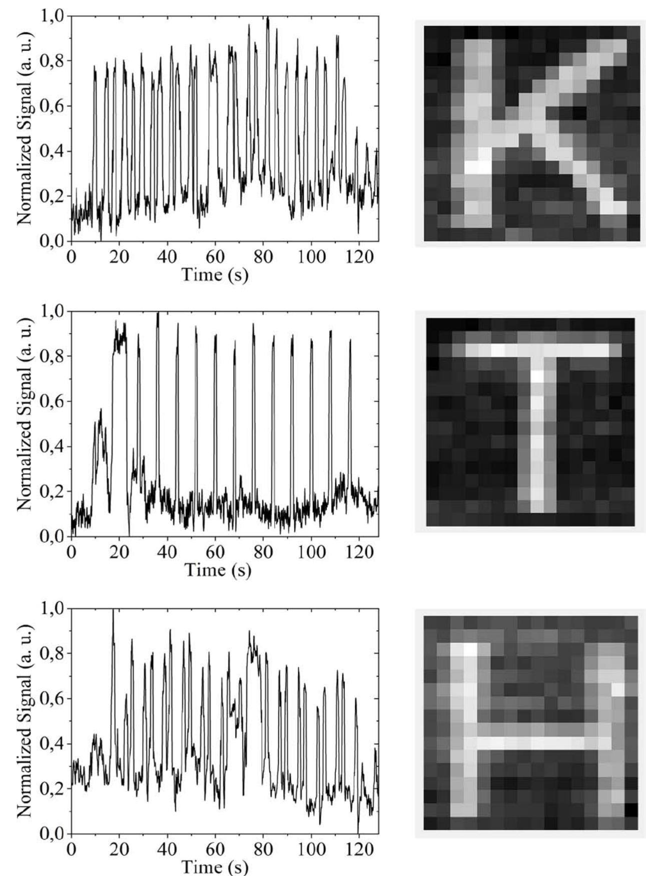

FIGURE 7. Normalized signals read-out from the image sensor and the 16×16 resolution grey-scale images converted from the signals at 400 °C. The light illuminated on the pixel sensors of the image sensor has spatial patterns ("K", "T", "H") masked from a UV LED.

photodiode due to a similar depletion (photon absorption) width. The transient response of the pixel sensor is shown in Fig. 4 (right). The inputs of R and C are programmed to have low voltage (0 V) and high voltage (10 V) at 1 Hz and 2 Hz respectively. Note that the OFF-state current is subtracted in Fig. 4 (d). The OFF-state current (both here and in the later results) is extracted as the minimum value of the current in the full measurement cycle. The read-out speed is limited by the parameter analyser with a 15 Hz sampling frequency.

To examine the two-level metal interconnect and signal uniformity from the pixels, a discrete 2×2 pixel sensor array was also tested. The transient response of the pixel sensor array with 2 row inputs and 2 column inputs (separated by two-level metal interconnect) is shown in Fig. 5. The waveforms of the four inputs are programmed to switch the four pixel sensors ON one after another with an total-OFF-state in between. The signal from the four pixels has a variation of ∼2%. The variation is consistent from RT to 400 °C, but not at 500 °C. The leakage current and photo-induced current from the transistors at 500 °C increase to be comparable to the photocurrent from the photodiode and are added into the output. This high temperature issue has also been found from the DC characteristics of the single pixel sensor in Fig. 4 (a).

B. IMAGE SENSOR

The characterization results of the basic gates, except for the tri-state buffer, used in the digital circuits have been reported in [28]. The measurement results of the tri-state buffer and the simulation results of the decoder and counter are reported in the Supplementary Material of this paper.

The image sensor was tested with the clock input of the counter at 2 Hz. The total current of the whole circuit at the ground terminal is around 0.55 A at RT. The current break-downs ∼0.2 A and ∼0.35 A to the pixel sensor array part and the digital part respectively. The total current increases around 10% at higher temperatures.

Three dark field Kapton masks with the patterns of letters "K", "T" and "H" were prepared by a laser cutter. Each mask was attached onto the pixel sensor array during measurement so that the light from the UV LED was shaded to have the corresponding geometrical pattern. The spatial response of the image sensor was recorded as the output current signal in time domain at RT (see Fig. 6) and 400 °C (see Fig. 7).

The signal was smoothed by the Savitzky-Golay (S-G) filter with a data segment length of 3 and then normalized, as expressed by Eq. (1)-(3).

$$S_{SG_i} = \left(S_{raw_{i-1}} + S_{raw_i} + S_{Raw_{i+1}}\right)/3 \quad (1)$$
$$S_i = S_{SG_i} - MIN(S_{SG}) \quad (2)$$
$$S_{norm_i} = S_i/MAX(S) \quad (3)$$

where S_{raw} is the raw signal, S_{SG} is the S-G filtered signal, S is the signal after baseline subtraction, S_{norm} is the final normalized signal.

Each normalized signal can be converted to a 16×16 resolution greyscale (1=white, 0=black) image, as also shown in Fig. 6 and Fig. 7. The images are able to display the different illumination conditions created by the masks.

The read-out signal has a fairly high noise even though the signal acquisition time is long. The noise is due to a small SNR, ∼2:1, of each pixel, as discussed above. Supposing 68 (for the case of "H") of all the 256 pixel sensors are illuminated by the light of the same intensity, the SNR of each illuminated pixel sensor in the whole array is only 69:68=1.015. The images taken at RT are sharper since less amount of thermal noise is generated at a lower temperature.

V. CONCLUSION

To conclude, we have demonstrated for the first time a SiC based 16×16 resolution image sensor circuit in bipolar technology. It is not only an original work in SiC opto-electronic on-chip integration, but also to date the most complex design of all existing SiC-based ICs. Taking advantage of the wide band gap of SiC, the image sensor is UV-only and it is able to operate up to 400 °C. The functionality of the image sensor has been verified by taking photos of spatial patterns masked from UV light. The image sensor is a promising demo for future high resolution, high temperature UV photography sensors, but three main challenges must be addressed: (1) The SNR of each pixel sensor should be optimized by eliminating the "hidden" photodiode in the current design. (2) The read-out speed should be improved by introducing a transimpedance amplifier and analogue-to-digital converter under the premise that the SNR of each pixel is enhanced. (3) Area and power consumption of the circuits should be reduced. CMOS is more suitable compared to TTL in this aspect. However, the thermal instability issue of the MOSFETs must be solved.

REFERENCES

[1] H. Pratt *et al.*, "UV imaging reveals facial areas that are prone to skin cancer are disproportionately missed during sunscreen application," *PLoS ONE*, vol. 12, no. 10, pp. 1–14, Oct. 2017, doi: 10.1371/journal.pone.0185297.

[2] P. Dondi, C. Invernizzi, M. Licchelli, L. Lombardi, M. Malagodi, and T. Rovetta, "Semi-automatic system for UV images analysis of historical musical instruments," in *Proc. Opt. Arts Archit. Archaeol. V*, vol. 9527, 2015, pp. 82–90, doi: 10.1117/12.2184744.

[3] A. V. Lindfors and L. Ylianttila, "Visualizing Rayleigh scattering through UV photography," *Bull. Amer. Meteorol. Soc.*, vol. 97, no. 9, pp. 1561–1564, 2016, doi: 10.1175/BAMS-D-14-00260.1.

[4] Z. Xu and B. M. Sadler, "Ultraviolet communications: Potential and state-of-the-art," *IEEE Commun. Mag.*, vol. 46, no. 5, pp. 67–73, May 2008, doi: 10.1109/MCOM.2008.4511651.

[5] T. Oshima, T. Okuno, N. Arai, N. Suzuki, H. Hino, and S. Fujita, "Flame detection by a β-Ga_2O_3-based sensor," *Jpn. J. Appl. Phys.*, vol. 48, no. 1, Jan. 2009, Art. no. 011605, doi: 10.1143/jjap.48.011605.

[6] J. L. Pau *et al.*, "Optical sensors based on III-nitride photodetectors for flame sensing and combustion monitoring," *Appl. Opt.*, vol. 45, no. 28, pp. 7498–7503, Oct. 2006, doi: 10.1364/AO.45.007498.

[7] J. Golimowski and K. Golimowska, "UV-photooxidation as pretreatment step in inorganic analysis of environmental samples," *Analytica Chimica Acta*, vol. 325, no. 3, pp. 111–133, 1996, doi: 10.1016/0003-2670(96)00034-7.

[8] J. L. Robichaud, "SiC optics for EUV, UV, and visible space missions," in *Proc. SPIE*, vol. 4854, 2003, pp. 39–49, doi: 10.1117/12.459771.

[9] A. Davies, Ed., *Digital Ultraviolet and Infrared Photography (1st Edition)*. Abingdon, U.K.: Routledge, 2017.

[10] *Wikipedia: Ultraviolet Photography*. Accessed: Oct. 10, 2019. [Online]. Available: https://en.wikipedia.org/wiki/Ultraviolet_photography

[11] E. Monroy, F. Omnès, and F. Calle, "Wide-bandgap semiconductor ultraviolet photodetectors," *Semicond. Sci. Technol.*, vol. 18, no. 4, p. R33, Mar. 2003, doi: 10.1088/0268-1242/18/4/201.

[12] P. G. Neudeck, "Progress in silicon carbide semiconductor electronics technology," *J. Electron. Mater.*, vol. 24, no. 4, pp. 283–288, Apr. 1995, doi: 10.1007/BF02659688.

[13] J. B. Casady and R. W. Johnson, "Status of silicon carbide (SiC) as a wide-bandgap semiconductor for high-temperature applications: A review," *Solid-State Electron.*, vol. 39, no. 10, pp. 1409–1422, 1996, doi: 10.1016/0038-1101(96)00045-7.

[14] D. T. Clark *et al.*, "High temperature silicon carbide CMOS integrated circuits," *Mater. Sci. Forum*, vol. 679, pp. 726–729, Mar. 2011, doi: 10.4028/www.scientific.net/MSF.679-680.726.

[15] N. Kuhns *et al.*, "Complex high-temperature CMOS silicon carbide digital circuit designs," *IEEE Trans. Device Mater. Rel.*, vol. 16, no. 2, pp. 105–111, Jun. 2016, doi: 10.1109/TDMR.2016.2530664.

[16] J. Holmes, A. M. Francis, I. Getreu, M. Barlow, A. Abbasi, and H. A. Mantooth, "Extended high-temperature operation of silicon carbide CMOS circuits for venus surface application," *J. Microelectron. Electron. Packag.*, vol. 13, no. 4, pp. 143–154, 2016, doi: 10.4071/imaps.527.

[17] P. G. Neudeck *et al.*, "Operational testing of 4H-SiC JFET ICs for 60 days directly exposed to venus surface atmospheric conditions," *IEEE J. Electron Devices Soc.*, vol. 7, pp. 100–110, 2019, doi: 10.1109/JEDS.2018.2882693.

[18] P. G. Neudeck, D. J. Spry, L. Chen, N. F. Prokop, and M. J. Krasowski, "Demonstration of 4H-SiC digital integrated circuits above 800 °C," *IEEE Electron Device Lett.*, vol. 38, no. 8, pp. 1082–1085, Aug. 2017, doi: 10.1109/LED.2017.2719280.

[19] M. Shakir, S. Hou, B. G. Malm, M. Östling, and C.-M. Zetterling, "A 600 °C TTL-based 11-stage ring oscillator in bipolar silicon carbide technology," *IEEE Electron Device Lett.*, vol. 39, no. 10, pp. 1540–1543, Oct. 2018, doi: 10.1109/LED.2018.2864338.

[20] R. Hedayati, L. Lanni, B. G. Malm, A. Rusu, and C. Zetterling, "A 500 °C 8-b digital-to-analog converter in silicon carbide bipolar technology," *IEEE Trans. Electron Devices*, vol. 63, no. 9, pp. 3445–3450, Sep. 2016, doi: 10.1109/TED.2016.2588418.

[21] Y. Tian and C.-M. Zetterling, "A fully integrated silicon-carbide sigma–delta modulator operating up to 500 °C," *IEEE Trans. Electron Devices*, vol. 64, no. 7, pp. 2782–2788, Jul. 2017, doi: 10.1109/TED.2017.2700632.

[22] L. C. Yu, G. T. Dunne, K. S. Matocha, K. P. Cheung, J. S. Suehle, and K. Sheng, "Reliability issues of SiC MOSFETs: A technology for high-temperature environments," *IEEE Trans. Device Mater. Rel.*, vol. 10, no. 4, pp. 418–426, Dec. 2010, doi: 10.1109/TDMR.2010.2077295.

[23] N. Kuhns *et al.*, "Complex high-temperature CMOS silicon carbide digital circuit designs," *IEEE Trans. Device Mater. Rel.*, vol. 16, no. 2, pp. 105–111, Jun. 2016, doi: 10.1109/TDMR.2016.2530664.

[24] S. Hou, P. E. Hellström, C. M. Zetterling, and M. Östling, "550 °C 4H-SiC p-i-n photodiode array with two-layer metallization," *IEEE Electron Device Lett.*, vol. 37, no. 12, pp. 1594–1596, Dec. 2016, doi: 10.1109/LED.2016.2618122.

[25] S. Hou, P.-E. Hellström, C.-M. Zetterling, and M. Östling, "Scaling and modeling of high temperature 4H-SiC p-i-n photodiodes," *IEEE J. Electron Devices Soc.*, vol. 6, no. 1, pp. 139–145, Dec. 2018, doi: 10.1109/JEDS.2017.2785618.

[26] S. Hou, P. E. Hellström, C. M. Zetterling, and M. Östling, "High temperature high current gain IC compatible 4H-SiC phototransistor," *Mater. Sci. Forum*, vol. 963, pp. 832–836, Sep. 2019, doi: 10.4028/www.scientific.net/MSF.963.832.

[27] S. Hou, P.-E. Hellström, C.-M. Zetterling, and M. Östling, "A 4H-SiC BJT as a switch for on-chip integrated UV photodiode," *IEEE Electron Device Lett.*, vol. 40, no. 1, pp. 51–54, Jan. 2019, doi: 10.1109/LED.2018.2883749.

[28] M. Shakir, S. Hou, R. Hedayati, B. G. Malm, M. Östling, and C.-M. Zetterling, "Towards silicon carbide VLSI circuits for extreme environment applications," *Electronics*, vol. 8, no. 5, p. 496, 2019, doi: 10.3390/electronics8050496.

[29] S. Hou, M. Shakir, P. Hellström, C. Zetterling, and M. Östling, "Process control and optimization of 4H-SiC semiconductor devices and circuits," in *Proc. Electron Devices Technol. Manuf. Conf. (EDTM)*, Mar. 2019, pp. 252–254, doi: 10.1109/EDTM.2019.8731140.

[30] H. Elahipanah, A. Asadollahi, M. Ekström, A. Salemi, C.-M. Zetterling, and M. Östling, "A wafer-scale Ni-salicide contact technology on n-type 4H-SiC," *J. Solid-State Sci. Technol.*, vol. 6, no. 4, pp. P197–P200, 2017, doi: 10.1149/2.0041705jss.

[31] M. Ekström, S. Hou, H. Elahipanah, A. Salemi, M. Östling, and C.-M. Zetterling, "Low temperature Ni-Al ohmic contacts to P-type 4H-SiC using semisalicide processing," *Mater. Sci. Forum*, vol. 6, pp. 389–392, Jun. 2018, doi: 10.4028/www.scientific.net/MSF.924.389.

[32] S. Hou, P. E. Hellström, C. M. Zetterling, and M. Östling, "4H-SiC PIN diode as high temperature multifunction sensor," *Mater. Sci. Forum*, vol. 897, pp. 630–633, Jun. 2017, doi: 10.4028/www.scientific.net/MSF.897.630.